

# The early- and late-time spectral and temporal evolution of GRB 050716

E. Rol,<sup>1\*</sup> J. P. Osborne,<sup>1</sup> K. L. Page,<sup>1</sup> K. E. McGowan,<sup>2</sup> A. P. Beardmore,<sup>1</sup>  
 P. T. O’Brien,<sup>1</sup> A. J. Levan,<sup>3</sup> D. Bersier,<sup>4</sup> C. Guidorzi,<sup>5</sup> F. Marshall,<sup>6</sup> A. S. Fruchter,<sup>4</sup>  
 N. R. Tanvir,<sup>1,3</sup> A. Monfardini,<sup>5</sup> A. Gomboc,<sup>5,7</sup> S. Barthelmy<sup>6</sup> and N. P. Bannister<sup>1</sup>

<sup>1</sup>University of Leicester, University Road, Leicester LE1 7RH

<sup>2</sup>School of Physics & astronomy, University of Southampton, Southampton SO17 3BJ

<sup>3</sup>Department of Physics, Astronomy and Mathematics, University of Hertfordshire, College Lane, Hatfield, Herts AL9 10AB

<sup>4</sup>Space Telescope Science Institute, 3700 San Martin Drive, Baltimore, MD 21218, USA

<sup>5</sup>Astrophysics Research Institute, Liverpool John Moores University, Twelve Quays House, Birkenhead CH41 1LD

<sup>6</sup>GSFC, USA

<sup>7</sup>Faculty of Mathematics and Physics, University of Ljubljana, Jadranska 19, 1000 Ljubljana, SI

Accepted 2006 October 23. Received 2006 October 23; in original form 2006 September 6

## ABSTRACT

We report on a comprehensive set of observations of gamma-ray burst 050716, detected by the *Swift* satellite and subsequently followed-up rapidly in X-ray, optical and near-infrared (NIR) wavebands. The prompt emission is typical of long-duration bursts, with two peaks in a time interval of  $T_{90} = 68$  s (15–350 keV). The prompt emission continues at lower flux levels in the X-ray band, where several smaller flares can be seen on the top of a decaying light curve that exhibits an apparent break around 220 s post-trigger. This temporal break is roughly coincident with a spectral break. The latter can be related to the extrapolated evolution of the break energy in the prompt  $\gamma$ -ray emission, and is possibly the manifestation of the peak flux break frequency of the internal shock passing through the observing band. A possible  $3\sigma$  change in the X-ray absorption column is also seen during this time. The late-time afterglow behaviour is relatively standard, with an electron distribution power-law index of  $p = 2$ ; there is no notable temporal break out to at least 10 d. The broad-band optical/NIR to X-ray spectrum indicates a redshift of  $z \gtrsim 2$  for this burst, with a host-galaxy extinction value of  $E_{B-V} \approx 0.7$  that prefers a small magellanic cloud (SMC)-like extinction curve.

**Key words:** radiation mechanisms: non-thermal – gamma-rays: bursts.

## 1 INTRODUCTION

One of the main goals of the *Swift* mission (Gehrels et al. 2004) is to obtain early-time information for gamma-ray burst (GRB) afterglows in X-ray and optical/ultraviolet (UV) wavelengths, using its rapid and autonomous slewing capability. In addition, longer term monitoring, especially in X-rays, has become more feasible than previously, with a dedicated facility like *Swift*.

Results of the early observations include the rapid decline of (X-ray) afterglows in the first tens of minutes (Tagliaferri et al. 2005; Goad et al. 2006). An explanation for this behaviour is prompt emission seen from angles further away from our line of sight (Kumar & Panaitescu 2000). It is likely that emission from the afterglow itself has not risen enough so early to contribute significantly to the measured flux, although there are some exceptions where the (X-ray) flux of the late-time external forward shock is already vis-

ible from early times on (e.g. O’Brien et al. 2006). A thorough understanding of this phenomenon requires detailed descriptions of the light curve (and broad-band spectral) behaviour early on, preferentially with as little as possible interference from other phenomena such as X-ray flares. These X-ray flares are seen in a number of bursts (e.g. Burrows et al. 2005a), and are now generally interpreted as continuing activity of the inner engine [King et al. 2005; but see also Piro et al. (2005), who interpreted the X-ray rebrightenings as the result of the beginning of the afterglow]. Late-time monitoring allows the construction of multiple epochs of combined near-infrared (NIR)/optical/UV and X-ray broad-band spectra (occasionally including radio data), building a more complete picture of GRB afterglows than before.

We present here a full analysis of GRB 050716. This includes the prompt (burst) emission in gamma-rays and early X-ray data, for which we performed time-resolved spectroscopy. We present the late-time X-ray behaviour of the afterglow, as well as late-time optical observations, which we then combine to form a broad-band spectrum. The observations and their analysis are described in

\*E-mail: er45@star.le.ac.uk

Section 2, and in Section 3 we discuss the results of the observations. In Section 4, we summarize our findings and draw our conclusions.

In the following,  $1\sigma$  errors are used except where noted. The temporal and spectral power-law indices  $\alpha$  and  $\beta$  are defined by  $F \propto t^{-\alpha} \nu^{-\beta}$ , and the photon index  $\Gamma = 1 + \beta$ . All *Swift* data have been reduced using the *Swift* software version 2.4 within the HEASOFT software (version 6.0.5) and the corresponding CALDB files.

## 2 OBSERVATIONS AND ANALYSIS

GRB 050716 was detected by the *Swift* Burst Alert Telescope (BAT; Barthelmy et al. 2005) on 2005 July 16, at 12:36:04 UT. All times mentioned in this text are relative to this  $T_0$ , except where noted. The spacecraft slewed and started observing in the X-ray and optical/UV bands 96 and 99 s later, respectively. The XRT (Burrows et al. 2005b) was able to immediately locate a position for the X-ray afterglow onboard, allowing ground-based telescopes to perform rapid, deep follow-up observations.

### 2.1 BAT analysis

BAT data were reduced using the BAT software tools within the *Swift* software package. A pulse height amplitude (PHA) to pulse height independent (PI) energy conversion was performed first with the BATECONVERT tool, which ensures the conversion is quadratic, rather than linear. We subsequently corrected the data for hot pixels. An additional systematic error correction was applied before spectral fitting. The 15–350 keV light curve is shown in Fig. 1.

The light curve shows an increase similar to the typical Fast-Rise Exponential-Decay (FRED) behaviour seen for many other bursts, with a peak around 9 s after trigger and the start of the rise of the light curve some 30 s earlier. A notable difference is that the rise is not as steep as usually seen for a FRED. A similar FRED light curve is superposed on the tail of the first one, producing a second peak 39 s after the trigger. After 80 s, most of the prompt emission has disappeared in the 15–350 keV energy band.  $T_{90}$  in this energy band for this burst is  $66 \pm 1$  s. A 4-s binned light curve shows some

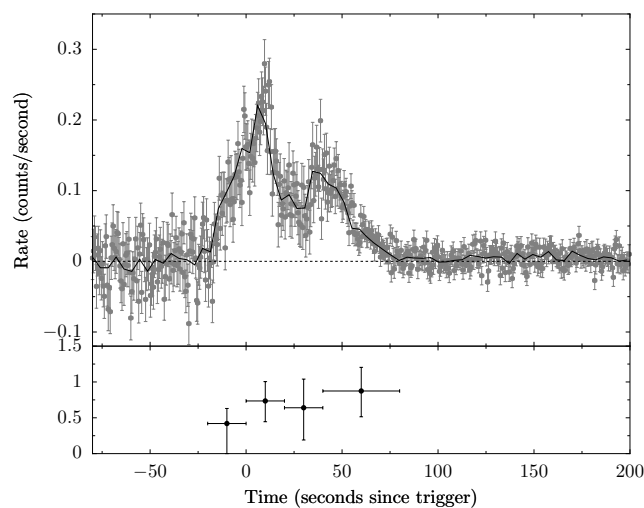


**Figure 1.** Top panel: the BAT 15–350 keV mask-weighted light curve, with the two peaks at around 9 and 39 s. Points are 0.5-s binned light curve, while the overplotted line is the 4-s binned light curve. The latter shows some evidence for possible emission after 80 s. Bottom panel: the spectral evolution of the prompt emission in the 15–150 keV range; shown is the photon index for a power-law model with an exponential cut-off.

**Table 1.** Results of spectral fits to four sections of the prompt gamma-ray emission, as well as that of the combined fit.

Section	Time (s)	$\Gamma$	Cut-off energy (keV)	$\chi^2_{\text{red}}$
A	–20–0	$0.42^{+0.21}_{-0.60}$	221 (> 6.7)	1.05
B	0–20	$0.74^{+0.27}_{-0.29}$	$125^{+178}_{-49}$	0.86
C	20–40	$0.64^{+0.40}_{-0.45}$	$105^{+305}_{-48}$	0.86
D	40–80	$0.87^{+0.33}_{-0.36}$	$65.6^{+47.5}_{-20.9}$	0.95
A–D	–20–80	$0.85^{+0.21}_{-0.23}$	$150^{+169}_{-54}$	0.76

emission still apparent past 80 s, up to 200 s, which is mostly found in the lower energy bands.

We have subdivided the gamma-ray data into four temporal sections and obtained spectral fits for each of these. The spectral shape was fitted with a power law, which results in an acceptable fit. A power law with an exponential cut-off, however, provides a better fit, while a fit with a Band model (Band et al. 1993) does not improve the fit compared to either one of those models. The BAT spectral energy range and low number of energy bins do not allow an accurate determination of the cut-off energy  $E_c$  in the cut-off power-law model (for the first section, it is in fact a lower limit), but there is an indication that the spectrum softens, with  $E_c$  gradually becoming lower, and the photon index  $\Gamma$  changing from about 0.4 to 0.9 during the prompt gamma-ray emission, over a period of  $\approx 50$  s.

To verify this spectral evolution, we have fitted the later time sections (C & D) with the model parameters (other than the normalization) fixed at those obtained from the earlier sections (A & B). By then freeing the parameters and applying an F-test, we find that there is indeed a change in the spectrum at a 99.9 per cent level. Performing a similar test to the first and last sections (A & D), with the results obtained from the fit to the total section (–20–80 s), also indicates a changing spectrum at a 99.9 per cent confidence level.

Such softening behaviour of the prompt spectrum has been commonly found before in other bursts (Ford et al. 1995). The results are detailed in Table 1, and include the result of a spectral fit to the whole time-span. Fig. 1 shows the spectral evolution of the prompt emission between 15 and 150 keV as well.

### 2.2 XRT analysis

XRT data were reduced from level 1 to 2 with the *Swift* software task XRTPIPELINE. Data obtained in Windowed Timing (WT) mode and Photon Counting (PC) mode have been used in all our following analysis. Counts were grouped by 20 per bin for the spectra. WT mode data for the light curve have been grouped by 40 counts per bin, and PC mode light curve data have been grouped by 20 counts per bin.

We have subdivided our analysis into an early-time part and a late-time part. We designate the early-time part as the section of the X-ray afterglow that shows flares (probably related to inner engine activity, see also the discussion below), while the late-time part shows a relatively smooth decay and is presumed to be the afterglow emission from a forward shock. The data for the early part extend up to almost 1 ks, with most of the data having been obtained in WT mode. The late-time part starts some 4 ks after the trigger and extends out to almost three weeks.

### 2.3 Early XRT data

WT mode observations started at 103 s, and extended up to 516 s. After this, the count-rate was low enough for the instrument to automatically switch to PC mode. WT mode data were extracted using a rectangular region with a length of 93 arcsec centred on the source and along the readout direction, with an equally sized region off-source serving as the background determination. PC mode data have been extracted with a 47 arcsec circular aperture instead of the default 71 arcsec, because of a contaminating close-by source. The first few 100 s of PC mode data are piled-up and we used an annular extraction region, with a 12-arcsec inner radius and a 47 arcsec outer radius. In addition, some bad columns are located near the source centre. We used default grades for WT mode (grades 0–2), while we used only grade 0 for the first few 100 s of PC-mode observations.

To determine the combined correction factor for the annular aperture and bad column loss, we modelled the PSF using XIMAGE, and calculated the ratio of the integrated response between an unmodified PSF and that masked out by an inner 12 arcsec circle and the bad columns. In the same manner, we correct for the expected loss of using only a 47 arcsec circular aperture. The combined correction factor is 4.47.

#### 2.3.1 Spectral evolution

Similar to the BAT observations, we find evidence for a change in the spectral slope over time. Modelling the spectrum with a simple power law, we find that the X-ray spectrum starts with  $\Gamma = 0.9 \pm 0.1$  (0.3–10 keV), and the slope then evolves to  $\Gamma = 2.0 \pm 0.1$ , with a change between 250 and 400 s post-trigger.

If a break is expected in the X-ray band, a broken power-law model for the spectra around this time is preferred. Fits with broken-power law models, however, do not show a significant improvement in the fit, and we have therefore used the results from the single power-law fits above.

Because there is still some flux in the BAT light curve coincident with the first 100 s or so of WT mode data, we have performed a joined fit to the BAT and XRT data between 100 and 200 s post-trigger. A single power-law fit has a  $\chi^2_{\text{red}}$  of 1.98 [degrees of freedom (DOF) = 61], but a Band model does a much better job ( $\chi^2_{\text{red}} = 0.90$ , DOF = 59) and results in  $E_0 = 12.2^{+5.4}_{-2.4}$  keV, or a peak energy of  $E_p = 13.1^{+5.8}_{-2.6}$  keV. The spectral indices are  $\alpha = -0.93^{+0.08}_{-0.13}$  and  $\beta = -2.56^{+0.37}_{-1.51}$ .

Because of the low number of counts in the BAT data, the fit is dominated by the XRT data and the outcome should be taken somewhat cautiously.

#### 2.3.2 Light curve

Since there is a change in the spectral slope halfway through the light curve, we cannot simply fit the count-rate light curve: a flux-calibrated light curve has to be used. To derive the count-rate to flux conversion factors, we have used the spectra between 103 and 223 s and between 263 and 513 s (see also Table 2), which provide the conversion values for the first and last part of the light curve, respectively. For the middle section, we have used the average of these values: the rapid change in spectrum does not allow for a good spectral fit. In all our following fits, we have modelled the two most pronounced flares with two simple Gaussians. We also left out the last data point of the light curve: it is likely that this point is the onset of the later time light curve (see Section 2.4), or possibly even the start of another flare.

**Table 2.** Results of spectral fits for the XRT WT mode data. The second half of the table details the results on variation of the column density (see also Fig. 3). A simple power law was used, with the Teubingen–Boulder model (Wilms, Allen & McCray 2000, TBABS) for the absorption.

Time (s)	$\Gamma$	$N_{\text{H}}$ ( $10^{21} \text{ cm}^{-2}$ )	$\chi^2_{\text{red}}$
103–123	$0.95 \pm 0.12$	$1.37^{+0.73}_{-0.66}$	0.509 (12.2/24)
123–143	$1.31^{+0.15}_{-0.14}$	$1.87^{+0.74}_{-0.67}$	0.899 (15.3/17)
143–163	$1.26 \pm 0.14$	$1.18^{+0.66}_{-0.61}$	0.518 (9.84/19)
163–183	$1.18^{+0.13}_{-0.12}$	$1.11^{+0.61}_{-0.57}$	0.698 (16.8/24)
183–243	$1.23 \pm 0.11$	$1.65^{+0.42}_{-0.39}$	0.801 (25.6/32)
243–363	$1.66 \pm 0.07$	$1.51^{+0.25}_{-0.23}$	1.09 (63.3/58)
363–403	$2.16^{+0.23}_{-0.21}$	$1.88^{+0.56}_{-0.53}$	1.12 (13.5/12)
403–513	$2.05^{+0.17}_{-0.16}$	$1.09^{+0.39}_{-0.36}$	1.09 (22.9/21)
<i>N<sub>H</sub> variation</i>			
103–223	$1.26 \pm 0.05$	$2.04^{+0.21}_{-0.20}$	0.890 (111.2/125)
263–513	$1.86^{+0.08}_{-0.07}$	$1.13^{+0.19}_{-0.18}$	1.053 (73.69/70)

A fit to the flux light curve with a single power law results in  $\chi^2_{\text{red}} = 2.06$  (DOF = 123), while a broken power-law fit gives  $\chi^2_{\text{red}} = 1.83$  (DOF = 121). Neither fit is good, but the broken power law does provide a significant improvement. A fit with a smoothly broken power law (either with the sharpness of the break fixed or free) hardly improves this ( $\chi^2_{\text{red}} = 1.78$  for both, DOF = 121 and 120, respectively), and an exponential fit is worse ( $\chi^2_{\text{red}} = 2.07$ , DOF = 123).

The broken power-law fit results in decay parameters  $\alpha_1 = 0.91^{+0.30}_{-0.09}$  and  $\alpha_2 = 3.78^{+0.19}_{-0.15}$ . The temporal break is found at  $220^{+27}_{-4}$  s, just before the time of the spectral break. This coincidence strengthens the suggestion that a broken power law is a reasonable model for the underlying light curve. See Section 3.1 for a more detailed exploration of this break.

The light curve and the spectral evolution are shown in Fig. 2. As commonly seen in other early X-ray light curves (e.g. Burrows et al. 2005a; Nousek et al. 2006; O’Brien et al. 2006), this one exhibits a few flares, which most likely indicates activity of the burst engine itself. This would agree with the possible emission seen in the BAT 15–350 keV range between 100 and 200 s. Also visible is the deviation of the underlying decay from a power law.

#### 2.3.3 X-ray absorption change?

For the combined WT mode data, we find no evidence for excess  $N_{\text{H}}$  above that of the estimated Galactic column of  $1.1 \times 10^{21} \text{ cm}^{-2}$  (Dickey & Lockman 1990). Subdividing the WT mode into a pre- and a post-spectral break section indicates, however, a modest amount of excess absorption at early times, while no excess absorption is measured past the break:  $N_{\text{H}} = 2.0(\pm 0.2) \times 10^{21}$  and  $1.1(\pm 0.2) \times 10^{21} \text{ cm}^{-2}$  for the total  $N_{\text{H}}$  at the two respective epochs. While the observed change in photon index could correlate with this change in  $N_{\text{H}}$ , a contour plot (Fig. 3) indicates it is likely that the column density did change. Something similar has been seen, for example, in the early (prompt) X-ray emission for GRB 000528 (Frontera et al. 2004), or claimed for GRB 050730 (Starling et al. 2005). An F-test for a model with  $N_{\text{H}}$  fixed at the later time value

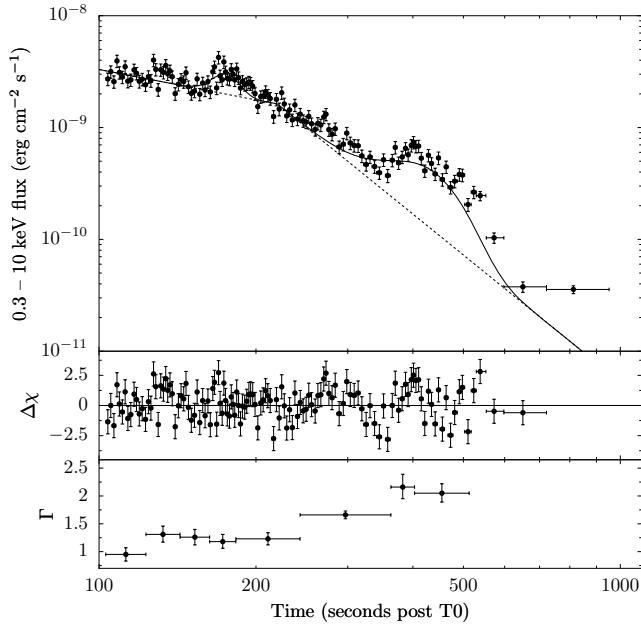


**Figure 2.** Top panel: 0.3–10 keV early-time light curve. The last three points are PC mode data, the previous data points consist of WT mode data. A broken power-law fit with two Gaussians is shown as the continuous line, with its break time around 200 s post-trigger. (The Gaussians account for the two main flares to obtain a better overall fit; the broken power law without Gaussians is shown as the dashed line.) The last data point has not been fit, since this likely belongs to the later time light curve. Middle panel: the fit residuals, expressed in sigma deviation. Even with the Gaussian fits to two flares, the overall light curve shows significant deviations from the fit. Bottom panel: the evolution of the photon index  $\Gamma$  of the X-ray spectrum.

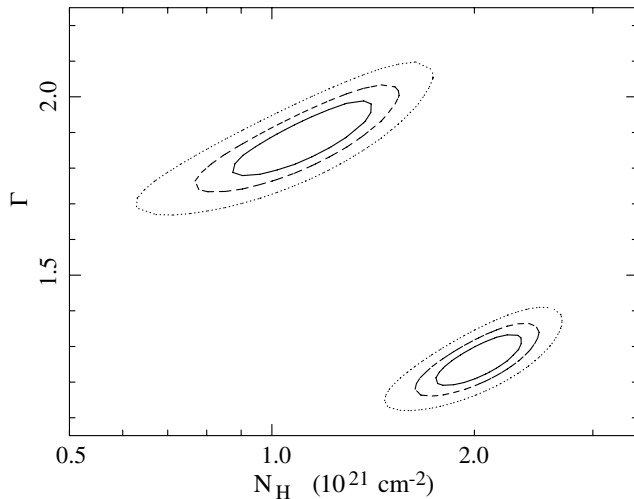


**Figure 3.** Contour plots for the  $1\sigma$ , 90 and 99 per cent combined confidence intervals for the photon index  $\Gamma$  and  $N_{\text{H}}$ . The contours upper-left are for the WT mode data after the observed spectral break (303–513 s), the contours in the lower right corner are pre-break (103–253 s). The middle part (253–303 s) is left out, since here the change in spectral break is most pronounced, indicating  $\Gamma$  is highly variable. Note that  $\Gamma$  for the first data section is slightly higher than the previously quoted 0.9, which is for the very first part of WT mode data only.

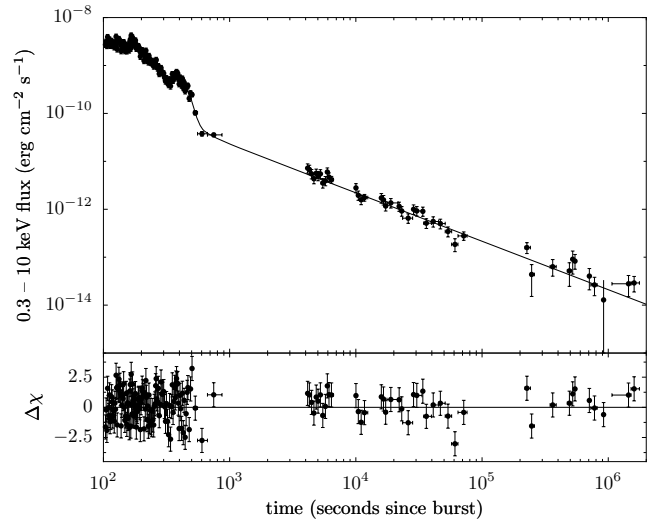


**Figure 4.** The complete X-ray light curve between 0.3 and 10 keV. The continuous line is modelled using a broken power law and two Gaussians for the early-time light curve (see Section 2.3), and a single power law added to that for the late-time light curve. The latter has a decay index of  $0.99 \pm 0.02$ . Bottom panel: the residuals of the fit, expressed in sigma deviation.

(see also Section 2.4), compared to a model with  $N_{\text{H}}$  free to fit, gives a probability of  $6.7e-5$  for the two models to be consistent (see the second part of Table 2 for more details).

## 2.4 Late-time XRT observations

The XRT data after 4 ks are not piled-up, and were extracted using a circular aperture of 47 arcsec radius and the default grades (0 to 12). The resulting 0.3–10 keV light curve follows a smooth power-law decline, with a power-law decay index of 0.99. The full light curve is shown in Fig. 4 and includes the early-time light curve as well. There is no indication of a shallow part ( $\alpha \lesssim 0.5$ ) in the light curve between the steep early decay and the later time decay, as often seen around this time in the light curve (e.g. Nousek et al. 2006); this may have been missed if it was relatively short and between the early- and late-time part. There has been, however, no need to include such a section in our fits to obtain good results. There is also no indication of a late-time break before the light curve is lost in the background noise, up to  $10^6$  s. A spectral fit to the data between 10 and 100 ks, with  $N_{\text{H}}$  fixed at its Galactic value, results in a good fit ( $\chi^2_{\text{red}} = 0.54$ ), with a photon index of  $\Gamma = 2.01^{+0.11}_{-0.10}$ .

## 2.5 Optical observations

Optical observations were automatically performed with the *Swift* Ultra Violet and Optical Telescope (UVOT; Roming et al. 2005) in the *UBVW1 M2 W2* filters and without a filter. The prompt dissemination of the position also triggered the Faulkes Telescope North (FTN), which began the first observations of its automatic follow-up procedure (Guidorzi et al. 2006) 243 s after the *Swift* trigger. Finally, NIR observations at the United Kingdom Infrared Telescope (UKIRT) started 56 min post-trigger, in the *JHK* bands, and Gemini NIRI *K*-band observations were obtained 22 h after  $T_0$ . The log of our observations can be found in Table 3.

A faint, fading source was detected in the UKIRT data, just outside the 90 per cent XRT error circle, and identified as the IR afterglow (Tanvir et al. 2005). The IR data also give the best position

**Table 3.** The results of our optical follow-up campaign covering the wavelength range from NIR to the near-UV. Other data collected through the GCN network provide only upper limits similar to those of the FTN and UVOT, and have therefore not been repeated here.

Start date (days UT, 2005 July)	Days since burst (mid-time)	Exposure time (s)	Filter	Magnitude	Telescope/instrument
16.529991	0.01954	400	<i>i'</i>	> 21.5	FTN
16.527721	0.00306	30	<i>R</i>	> 20.3	FTN
16.527721	0.02239	540	<i>R</i>	> 22.3	FTN
16.529911	0.02236	520	<i>B</i>	> 23.0	FTN
16.526169	0.4315	5799	<i>V</i>	> 21.2	<i>Swift</i> /UVOT
16.527859	0.4042	5507	<i>B</i>	> 22.1	<i>Swift</i> /UVOT
16.527697	0.3988	5477	<i>U</i>	> 21.6	<i>Swift</i> /UVOT
16.527534	0.4416	5053	<i>W1</i>	> 21.5	<i>Swift</i> /UVOT
16.527373	0.4374	5486	<i>M2</i>	> 21.8	<i>Swift</i> /UVOT
16.528044	0.4084	4383	<i>W2</i>	> 21.8	<i>Swift</i> /UVOT
19.055751	2.7699	9480	'white'	> 22.5	<i>Swift</i> /UVOT
16.579109	0.05594	300	<i>J</i>	20.76 ± 0.08	UKIRT/UFTI
16.581678	0.05937	450	<i>H</i>	19.31 ± 0.05	UKIRT/UFTI
16.564178	0.04272	600	<i>K</i>	17.74 ± 0.15	UKIRT/UFTI
16.583727	0.06055	300	<i>K</i>	18.22 ± 0.15	UKIRT/UFTI
17.421337	0.9275	3600	<i>K</i>	20.5 ± 0.2	Gemini/NIRI

for the GRB and its afterglow. This is RA = 22:34:20.73, Dec. = +38:41:03.6 (J2000), with an estimated error of 0.4 arcsec. This position is derived from the NIRI *K*-band image, calibrated with respect to the Two-Micron All Sky Survey (2MASS) survey (Skrutskie et al. 2006).

A single power-law fit to the three *K*-band points results in a power-law decay index of  $\alpha_o = 0.80^{+0.13}_{-0.07}$ , with  $\chi^2_{\text{red}} = 0.689$ . While different from the X-ray decay slope at these times, the paucity of data points does not allow a strong quantification of this difference. A fit with  $\alpha_o$  fixed at  $\alpha_X = 0.99$ , however, results in  $\chi^2_{\text{red}} = 2.58$ .

We calculated the *JHK* spectral index by shifting the data to a common epoch using the previously calculated decay index, and correcting for the estimated Galactic extinction (Schlegel, Finkbeiner & Davis 1998). Conversion to flux was performed using the Vega fluxes from Fukugita, Shimasaku & Ichikawa (1995) for the optical and from Tokunaga & Vacca (2005) for the NIR filters. The fit shows the spectrum to be inconsistent with a power-law spectrum ( $\beta_o = 2.9$ , but  $\chi^2_{\text{red}} = 4.2$ ), indicative of intrinsic reddening. We address this in Section 3.2.

### 3 DISCUSSION

Here we discuss the results obtained above. A short summary of the results is given in Table 4.

**Table 4.** Summary of the main results obtained in Section 2. We have converted the spectral results from  $\Gamma$  to  $\beta$ .

Data section	$\beta$	$\alpha$
X-ray, 103–223 s	0.26 ± 0.05	0.91 $^{+0.30}_{-0.09}$
X-ray, 263–513 s	0.86 $^{+0.08}_{-0.07}$	3.78 $^{+0.19}_{-0.15}$
X-ray, post 1 h	1.01 $^{+0.11}_{-0.10}$	0.99 ± 0.02
optical, post 1 h	2.94 <sup>1</sup>	0.80 $^{+0.13}_{-0.07}$

<sup>1</sup>  $\chi^2_{\text{red}} = 4.2$ , therefore no error has been calculated

#### 3.1 Early emission

GRB 050716 shows characteristics as seen in previous (*Swift*) bursts, both in its prompt emission and the (early) afterglow (Nousek et al. 2006; O’Brien et al. 2006). The flares, combined with the multiple peaks in the gamma-ray emission, imply several shocks, likely indicative of prolonged engine activity (King et al. 2005). The early X-ray data show a power-law decline that appears to be unrelated to the later afterglow emission and which is often explained as prompt emission originating from higher latitudes at the emission source, after the emission at smaller angles has faded away.

In the context of this model, we can test the curvature effect  $\alpha = 2 + \beta$  (Kumar & Panaitescu 2000). We used the values pre- and post-break in the XRT data, showing that by this relation, the observed  $\alpha_1$  is too shallow and  $\alpha_2$  too steep. Zhang et al. (2006) list several possible causes why this relation would not hold. Most important are the effect of using the trigger time instead of the time of the last emission peak (thereby assigning an incorrect zero-point for a power-law fit), and that of superposition of tails of several emission peaks. Both causes could be valid here since the last significant emission peaks some 40 s after the trigger. However, applying such a correction for both effects would effectively produce an ever shallower decay, making the discrepancy larger. Possible causes for  $\alpha$  being too shallow are the fact that one is looking at a structured jet (Rossi, Lazzati & Rees 2002) or when the observed (X-ray) wavelength regime is still below the cooling break. In the latter case, the decay is given by  $\alpha \sim 1 + 3\beta/2$  (Zhang et al. 2006). Only the very early section of the X-rays agrees with this relation, with  $\alpha = 0.91$  and  $\beta = -0.1$  (Section 2.3.2, Table 2). Post-break, however, the discrepancy is even larger in this scenario. Potentially, both the peak frequency and the cooling break have passed the X-ray band at this time. While this could explain the relatively long spectral transition, there is no direct evidence for this. The discrepancy at later times, for either relation, might more likely be attributed to an increasing influence of the external shock (which likely dominates the last data), and the last flare, which hampers a good fit to the steeper tail of the early light curve.

Evolution of the early emission in the X-ray to gamma-ray energy range has been studied before, for example, by Frontera et al. (2000), who looked at the spectral evolution for eight *BeppoSAX* bursts which had been detected by both the Gamma Ray Burst Monitor (GRBM) and one of the wide field cameras (WFCs). While their findings are similar, an important advantage here is that we have an early X-ray light curve which, with provisions for some flaring, can be fit with a broken power law; the break time of this power law is roughly coincident with the moment  $E_p$  passes through the X-ray band. The WFC data generally cover only the very early part of the burst, and any underlying (broken) power law is not visible. As a result, the  $E_p$  evolution could only be deduced from the spectral changes for the *BeppoSAX* data.

Variable X-ray absorption at early times in the X-ray spectra of GRBs has been noted before in other GRBs (Amati et al. 2000; Frontera et al. 2000; in't Zand et al. 2001; Starling et al. 2005). Lazati & Perna (2002) have suggested that ionization strongly modifies the absorption properties of the surrounding material. For this effect to be notable, the material should be in a compact region surrounding the GRB ( $< 5$  parsec), and have an initial column density  $N_H > 10^{21} \text{ cm}^{-2}$ . The change detected here is  $0.8 \times 10^{21} \text{ cm}^{-2}$  at redshift 0. For a redshift of  $z = 2$  (see below), the column density would be  $N_H \approx 1.5 \times 10^{22} \text{ cm}^{-2}$  (at solar metallicity), large enough to fulfil the  $N_H > 10^{21} \text{ cm}^{-2}$  criterion.

### 3.2 The late-time light curve and broad-band spectrum

From the combination of the X-ray temporal and spectral index around 5 ks, we can infer an electron power-law index of  $p = 2.0$  within the standard fireball model (e.g. Mészáros & Rees 1997; Chevalier & Li 1999; Sari, Piran & Halpern 1999). This assumes that (i) the afterglow is in the slow-cooling regime ( $v_m < v_c$ ), (ii)  $v_c$  is below the X-rays and (iii) the jet-break has not manifested itself at this time. Other scenarios are easily ruled out by invalidating relations between the two indices (see e.g. table 1 in Zhang & Mészáros 2004). There is still a degeneracy between the type of circumburst environment [a constant density medium or a medium with a  $R^{-2}$  dependency ( $R$  the distance from the centre) such as a stellar wind], which can potentially be resolved by looking at the temporal and spectral indices below  $v_c$ ; in our case the only candidate for that is the optical band, which is generally found to be below  $v_c$  at these times. To verify whether this is indeed the case, we compared the X-ray and optical decay indices.

There is a  $1.5\sigma$  difference between the afterglow decay slope in optical and X-rays, which is only marginally significant and does allow  $v_c$  to be below optical wavelengths. However, a cooling break between the optical and X-ray waveband makes the picture self-consistent: for an interstellar medium (ISM)-like, the decay index in optical should be 0.25 lower than that in X-ray, 0.74, which is certainly compatible with  $\alpha_o$  obtained from our fit to the  $K$ -band data. On the other hand, for a wind-like medium, the optical decay index would have to be 0.25 higher than that in X-ray, 1.24, and is therefore incompatible with  $\alpha_o$ .

The non-power-law behaviour of the NIR spectrum indicates reddening, which we estimate by examining the broad-band spectral behaviour, by combining the X-ray, optical and NIR data. For this, we have extrapolated the optical and X-ray data to a common epoch: we choose 0.04 d (3.5 ks) after trigger, which is central to the optical FTN and NIR UKIRT data, and lies just at the beginning of the late-time X-ray data. We obtained an unabsorbed X-ray flux from the data between 4 and 12 ks (orbits 2 and 3 combined), which were then extrapolated back to 0.04 d using the power-law decay index

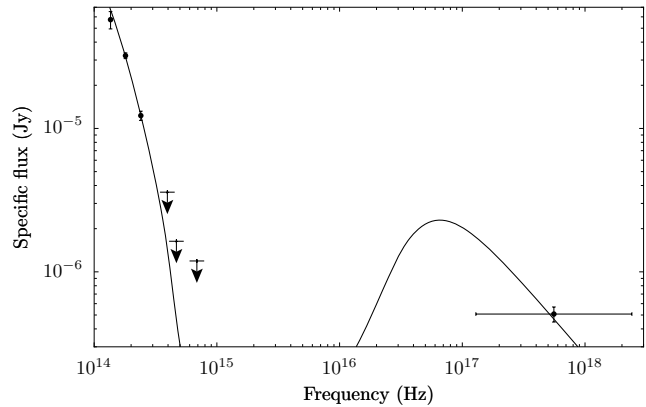


**Figure 5.** The X-ray to optical/NIR broad-band spectrum of GRB 050716, 0.04 d post-burst. The best fit is shown for a broken power law connecting the two wavelength ranges, with host-galaxy absorption for a SMC-like extinction curve at  $z = 2$ . The X-ray spectrum has been represented relatively simply by a single data point. This has the purpose of enhancing the  $\chi^2_{\text{red}}$  sensitivity on the NIR data instead of on the X-ray data, since we try to calculate the estimated optical/UV host-galaxy extinction.

of 0.99. The optical and NIR data were corrected for Galactic extinction and converted to fluxes as before. We then extrapolated to 0.04 d post-trigger using our estimate for the optical power-law decay index.

With the scaled fluxes, we constructed the broad-band spectrum of GRB 050716 at 0.04 d (Fig. 5). We then tried to fit the data with models available within the standard fireball model, allowing for intrinsic (UV/optical) extinction within the host galaxy and a Lyman cut-off resulting from its redshift. No spectroscopic redshift is known, however. While in principle one can obtain a photometric redshift, there are too many free parameters with the few available data to do this accurately. We have therefore obtained an estimate of the intrinsic extinction for an afterglow positioned at various redshifts (1, 2, 3, ..., 7). We have further constrained the power-law slope connecting the X-ray and optical/NIR regime to be equal to that obtained by the X-ray spectral fit alone,  $\beta = 1.0$ .

A single power law, absorbed by host-galaxy extinction or intergalactic Lyman extinction, is not able to reproduce the observed broad-band spectrum. A spectral break between optical and X-ray is required, as already found from the fits to the optical and X-ray light curves. With the assumption that this break is indeed the cooling break (with  $\Delta\beta = 0.5$ , we have kept the lower end of this break fixed at a power-law index of  $\beta_{\text{opt}} = 0.5$ , and the higher end at  $\beta_X = 1.0$ ). Reasonable fits are then obtained for redshifts above  $z = 2$ , with host-galaxy extinction that follows a small magellanic cloud (SMC)-like extinction curve ( $E_{B-V} = 0.5-0.7$ ,  $A_V = 1.5-2.1$ , with lower values for higher redshifts (see Fig. 5). This estimate for the host-galaxy is higher than on average found for GRB host galaxies, but not unknown (e.g. Levan et al. 2006). However, localized extinction or a line-of-sight through an edge-on galaxy could easily explain the somewhat larger than average host extinction.

The reduced  $\chi^2$  is in all cases  $\lesssim 1$  (for redshifts above 4, it becomes much less than 1), resulting in a lower limit on the redshift of  $z \gtrsim 2$ . A Galactic-type extinction curve results in a steeper NIR slope than measured here, and provides a worse fit. The same gradual NIR slope also implies that host-galaxy extinction should be present, and cannot be explained by a Lyman break alone. We further looked at the resultant extinction value for small changes ( $\pm 0.1$ ) in our assumed spectral index, which results in changes of about 0.1 mag

in  $E_{B-V}$ . (The value for  $\chi^2_{\text{red}}$ , however, also increases considerably doing so.) Finally, from our best fit we find that the  $\nu_c$  cannot be located directly below the X-ray frequencies, but is restricted to  $\sim 10^{16}$  Hz.

An  $E_{B-V}$  of 0.7 with a SMC-like extinction curve would imply an  $N_{\text{H}}$  of  $3.2 \times 10^{22}$  (Martin, Maurice & Lequeux 1989) in the host galaxy. Correcting for an assumed SMC metallicity of 1/4 solar and adjusting for the redshift of  $z = 2$ , this turns out to be not measurable above the estimated Galactic extinction in our data, and indeed, no excess extinction is measured past 300 s.

We can obtain a lower limit on the fluence and burst energy from the BAT spectrum, which results in  $5.9 \times 10^6$  erg  $\text{cm}^{-2}$  and  $5.6 \times 10^{52}$  erg, respectively. Both values are in the 15–150 keV energy range in the observer's frame. With a lower limit of  $z \gtrsim 2$ , the relation found by Amati (Amati et al. 2002; Amati 2006) gives  $E_p \gtrsim 76$  keV in the observers frame, while we find  $E_p \gtrsim 170$  keV from the spectral fit (Table 1, after conversion of the cut-off energy to  $E_p$ ). Note that the latter uses a power law with an exponential cut-off, not the Band function. Using the previous fit values with a Band function, fixing  $\beta = -2$ , and extrapolating outside the BAT spectral range (0.001–10<sup>4</sup> keV), we obtain an estimate of the isotropic energy of  $E_{\text{iso}} \approx 2.3 \times 10^{53}$  erg, which is almost four times larger than the 15–150 keV estimate. Using the Amati relation, this would put the peak energy at  $\sim 150$  keV in the observer frame, assuming  $z \approx 2$ . This redshift estimate therefore agrees reasonably well with the results expected from the Amati relation, and indicates  $z \approx 2$  is a likely good estimate for the redshift of this burst.

#### 4 SUMMARY

We have presented here a comprehensive analysis of the data available on GRB 050716. The most remarkable feature of the early emission is the spectral change, clearly visible in the X-rays, which can possibly be traced back to the gamma-ray emission. The temporal break coincident with the spectral break points to the peak-flux frequency passing through the X-rays at this time. In addition, the X-ray absorption before the break appears to be larger than after the break. While this could be an artificial result related to the break, care has been taken to eliminate instrumental effects and the result appears to be significant, possibly indicating ionization of surrounding medium.

At later times, our multi-wavelength data of GRB 050716 show a fairly standard afterglow: the X-ray light curve and spectrum indicate  $p = 2$ , with no evidence for a break related to the broadening of the jet outflow. The optical data are rather limited, partly because the optical afterglow is relatively faint: host-galaxy extinction with  $A_V = 1.5$ –2.1 can account for the obtained upper limits. Though no spectroscopic redshift has been obtained for GRB 050716, we obtain a lower limit of  $z \gtrsim 2$ , which appears to be in agreement with the Amati relation.

#### ACKNOWLEDGMENTS

We thank the referee for a careful reading of the manuscript, which improved it overall. ER, JPO, KLP, APB, AJL and NRT acknowledge financial support from PPARC. The authors like to thank

Simon Vaughan for additional help with parts of the data analysis. This work is also supported at Pennsylvania State University (PSU) by NASA contract NAS5-00136 and NASA grant NNG05GF43G, and at the Osservatorio Astronomico di Brera (OAB) by funding from ASI on grant number I/R/093/04. 'The UKIRT is operated by the Joint Astronomy Centre on behalf of the UK Particle Physics and Astronomy Research Council.' This publication makes use of data products from the 2MASS, which is a joint project of the University of Massachusetts and the Infrared Processing and Analysis Centre/California Institute of Technology, funded by the National Aeronautics and Space Administration and the National Science Foundation. We gratefully appreciate the contributions of all members of the *Swift* team.

#### REFERENCES

- Amati L., 2006, MNRAS, 372, 233  
 Amati L. et al., 2000, Sci, 290, 953  
 Amati L. et al., 2002, A&A, 390, 81  
 Band D. et al., 1993, ApJ, 413, 281  
 Barthelmy S. D. et al., 2005, Space Sc. Rev., 120, 143  
 Burrows D. N. et al., 2005a, Sci, 309, 1833  
 Burrows D. N. et al., 2005b, Space Sci. Rev., 120, 165  
 Chevalier R. A., Li Z., 1999, ApJ, 520, 29  
 Dickey J. M., Lockman F. J., 1990, ARA&A, 28, 215  
 Ford L. A. et al., 1995, ApJ, 439, 307  
 Frontera F. et al., 2000, ApJS, 127, 59  
 Frontera F. et al., 2004, ApJ, 614, 301  
 Fukugita M., Shimasaku K., Ichikawa T., 1995, PASP, 107, 945  
 Gehrels N. et al., 2004, ApJ, 611, 1005  
 Goad M. R. et al., 2006, A&A, 449, 89  
 Guidorzi C. et al., 2006, PASP, 118, 288  
 in't Zand J. J. M. et al., 2001, ApJ, 559, 710  
 King A., O'Brien P. T., Goad M. R., Osborne J., Olsson E., Page K., 2005, ApJ, 630, L113  
 Kumar P., Panaitescu A., 2000, ApJ, 541, L51  
 Lazzati D., Perna R., 2002, MNRAS, 330, 383  
 Levan A. et al., 2006, ApJ, 647, 471  
 Martin N., Maurice E., Lequeux J., 1989, A&A, 215, 219  
 Mészáros P., Rees M. J., 1997, ApJ, 476, 232  
 Nousek J. A. et al., 2006, ApJ, 642, 389  
 O'Brien P. T. et al., 2006, ApJ, 647, 1213  
 Piro L. et al., 2005, ApJ, 623, 314  
 Roming P. W. A. et al., 2005, Space Sci. Rev., 120, 95  
 Rossi E., Lazzati D., Rees M. J., 2002, MNRAS, 332, 945  
 Sari R., Piran T., Halpern J. P., 1999, ApJ, 519, 17  
 Schlegel D. J., Finkbeiner D. P., Davis M., 1998, ApJ, 500, 525  
 Skrutskie M. F. et al., 2006, AJ, 131, 1163  
 Starling R. L. C. et al., 2005, A&A, 442, L21  
 Tagliaferri G. et al., 2005, Nat, 436, 985  
 Tanvir N. et al., 2005, GCN Circ., 3632, 1  
 Tokunaga A. T., Vacca W. D., 2005, PASP, 117, 421  
 Wilms J., Allen A., McCray R., 2000, ApJ, 542, 914  
 Zhang B., Fan Y. Z., Dyks J., Kobayashi S., Mészáros P., Burrows D. N., Nousek J. A., Gehrels N., 2006, ApJ, 642, 354  
 Zhang B., Mészáros P., 2004, Int. J. Modern Phys. A, 19, 2385

This paper has been typeset from a  $\text{\TeX}/\text{\LaTeX}$  file prepared by the author.